ISBN: 978-3-95450-211-0 doi:10.18429/JACoW-SRF2019-TUP056

A FIRST-PRINCIPLES STUDY ON MAGNETIC FLUX TRAPPING AT NIOBIUM GRAIN BOUNDARIES

P. Garg[1], L. Cooley[2], T. R. Bieler[3] and K. N. Solanki[1*]
[1]School for Engineering of Matter, Transport, and Energy, Arizona State University, Tempe, AZ, USA
[2]Applied Superconductivity Center, National High Magnetic Laboratory, Tallahassee, FL, USA
[3]Department of Material Sciences and Engineering, Michigan State University, East Lansing, MI, USA

Abstract

Superconducting radio frequency cavities are primarily fabricated from niobium. The superconducting material expels the external magnetic field, while operating in Meissner state. However, due to defects such as grain boundaries, the field can be pinned in the material even after the external field is removed, thereby reducing the effectiveness of niobium. The mechanism for such behavior is unknown; therefore, first-principles methods were used to gain a theoretical perspective on the role of grain boundaries on magnetic flux trapping. The external magnetic field was simulated within the first-principles framework along the grain boundaries to determine their flux trapping tendencies. The results clearly demonstrate a significant amount of trapped flux and the electronic structure of defects was observed to be significantly different from bulk niobium. Overall, defects and their interaction with the external magnetic field leads enhanced non-paramagnetic behavior in niobium.

INTRODUCTION

Superconducting radio-frequency (SRF) cavities, one of the critical components to develop high-performance particle accelerators, are primarily fabricated from niobium [1,2]. SRF cavities are operated in the Meissner state such that an external magnetic field is expelled from the superconducting material [3]. However, the presence of material imperfections like defects, impurities etc. can suppress the expulsion of magnetic field and pin the field inside the material even after the externally applied field is removed [4,5]. The performance of SRF cavities is measured in terms of the quality factor $Q_O = G/R_S$, where the geometric factor G depends on the cavity geometry and R_S is the surface resistance of the inner cavity wall [6,7]. The surface resistance (R_S) comprises of the Bardeen-Cooper-Schrieffer (BCS) resistance R_{BCS} and the residual surface resistance R_{res} [8,9]. The R_{res} arises from magnetic flux trapping, normal conducting precipitates, impurities, defects etc., which depend on the material properties [10,11]. The major contribution to R_{res} stems from magnetic flux trapping at defects during cavity cooling [12,13] and therefore it is critical to reduce the trapped magnetic flux in order to improve Q_O of niobium SRF cavities.

The flux trapping at the crystal lattice imperfections like dislocations and grain boundaries contribute to R_{res} and degrade the performance of niobium for SRF applications [14–16]. Aull *et al.* [17] reported nearly 100% flux trapping in polycrystalline niobium, which decreased to ~41% in heat treated, and polished single crystal niobium samples. Flux pinning at the grain boundaries in niobium bi-crystals was found to be dependent upon the grain boundary tilt axis and attributed to the electron-scattering mechanism [18,19]. Additionally, flux trapping due to hydride segregation along the low angle grain boundaries has also been reported during magneto-optical imaging analysis [20]. Several theories such as crystal-anisotropy of the upper critical field [21,22], electron-scattering at the grain boundary [19], elastic interactions between the dislocations present at the grain boundaries and the flux line lattice [23] etc. had been proposed to explain the flux trapping at defects. However, mechanism(s) underlying the flux pinning at defects has not been unequivocally established since the applicability of various flux pinning theories at defect has not been determined for a wide variety of samples.

This work marks the first attempt to understand the influence of grain boundaries on magnetic flux trapping in niobium within the first-principles framework. Equilibrium structures for Σ5(210) and Σ5(310) grain boundaries were obtained using molecular dynamics and density functional theory calculations. The external magnetic field was simulated using the all-electron full-potential linearized augmented plane wave code to analyze the flux trapping tendencies of planar defects in niobium. Grain boundary character was found to play a crucial role on the flux trapping behavior since the trapped flux was observed to vary with the grain boundary mis-orientation angle. To determine the mechanisms underlying the interactions between external magnetic field and grain boundaries, the electronic structure of defects was analyzed using electronic density of states and Bader charge analysis within first-principles framework. Differences in the electronic structure of defects as compared to bcc niobium indicate to a potential magnetic state in the presence of an external magnetic field thereby promoting flux trapping at grain boundaries in niobium. Such information will provide guidance for developing processing techniques to minimize undesirable boundaries and improve the quality factor of niobium SRF cavities.

COMPUTATIONAL METHODOLOGY

The first-principles calculations were performed within density functional theory (DFT) framework using Vienna

*email: kiran.solanki@asu.edu

ISBN: 978-3-95450-211-0 doi:10.18429/JACoW-SRF2019-TUP056

Ab-initio Simulation Package (VASP) [24]. The projector augmented wave (PAW) pseudopotentials with Perdew-Burke-Ernzerhof (PBE) [25,26] exchange-correlation formulation were used to represent niobium with the valence 5s, 4d, and six of the 4*p* electrons. A plane wave basis set with an energy cutoff of 550 eV was used to represent the wave function with a Monkhorst Pack *k* point mesh, selected after extensive convergence studies for different defect structures to carry out the Brillouin-zone integrations [27]. The computed niobium lattice parameter of 3.31 Å and other equilibrium structure parameters like elastic constants were found to match very well with the previously reported experimental and theoretical values [14].

The state-of the-art all-electron full-potential linearized augmented plane wave (FP-LAPW) code was used to analyze the flux trapping behavior of defects in niobium [28]. The FP-LAPW code formulation is based on the Kohn-Sham equations for external field in a two-step process [28-30]. In the first-variational step a Hamiltonian ($\hat{H}$) containing only the scalar potential and **E** field is constructed

$$\hat{H} = \hat{T}_s + \hat{V}_{ext} + \boldsymbol{E}.\hat{\boldsymbol{r}} + \hat{V}_{xc} \qquad (1)$$

and diagonalised with $\hat{H}|\phi_i\rangle = \varepsilon_i|\phi_i\rangle$. $\hat{T}_s$ represents the kinetic energy, $\hat{V}_{ext}$ is the external potential, $\hat{V}_{xc}$ is the exchange-correlation (XC) potential and ε_i is the orbital energy of the corresponding Kohn–Sham orbital, ϕ_i [28]. In the second-variational step, the magnetic fields, spin-orbit coupling and **A** field are added using the first-variational step as a basis

$$H_{ij} = \varepsilon_i\delta_{ij} + \langle\phi_i|\boldsymbol{\sigma}\cdot\left(\hat{\boldsymbol{B}}_{\boldsymbol{ext}} + \hat{\boldsymbol{B}}_{\boldsymbol{xc}}\right) + \boldsymbol{\sigma}\cdot\hat{L} + \boldsymbol{A}\cdot\hat{\boldsymbol{\nabla}}\,|\phi_i\rangle \qquad (2)$$

where B_{xc} is the XC magnetic field. Instead of the usual approach of separating the Kohn-Sham equations into spin-up and spin-down orbitals, densities and potentials, the FP-LAPW code formulation treats magnetism as non-collinear for which the basic variables are the scalar density ρ(r) and the magnetization vector field m(r). An external magnetic field (B_{ext} = 171.5 mT) was applied along different defects, below superconducting transition temperature of niobium (T_c = 9.25 K), during the flux trapping calculations. Periodic boundary conditions were maintained along all directions. The applied field was decreased by a factor of 0.85 after each self-consistent loop such that the applied field is infinitesimal at the end of all loops. The self-consistent loop converged when the total energy is $<10^{-3}$ eV and the root mean square change in Kohn-Sham potential and magnetic field is $<10^{-3}$ Tesla.

Molecular dynamics (MD) simulations were used to model the equilibrium grain boundary (GB) structures using empirical interatomic potentials. <100> symmetric tilt grain boundary (STGB) systems were created in Large-scale Atomic/Molecular Massively Parallel Simulator (LAMMPS) [31] with semi-empirical embedded atom method (EAM) potential for niobium. The equilibrium grain boundary structures were determined using a bi-crystal simulation cell with 3D periodic boundary conditions and sufficiently large grains in the perpendicular direction to obtain minimum energy GB structures (see Figure 1a) [32-35]. For instance, the Σ5(210) niobium grain boundary was modeled by two (210) oriented slabs of Nb each, reflected with respect to the xz-plane followed by an atom deletion technique and energy minimization using a nonlinear conjugate gradient method (see Figure 1b) [36-38]. All atoms of the GB supercells were allowed to relax to an energy convergence of $<10^{-6}$ eV [39]. The grain boundary energy (E_{gb}) was calculated as the difference between the energy of the GB simulation cell with n atoms (E_n) and the cohesive energy of niobium atoms (E_{coh}) per unit area of the grain boundary plane (A).

$$E_{gb} = \frac{E_n - n*E_{coh}}{2A} \qquad (3)$$

The expression is divided by 2 due to the two interfaces in the grain boundary simulation cell. The GB energy as a function of the mis-orientation angle for ⟨100⟩ tilt axes of niobium is shown in Fig. 1a. Furthermore, Fig. 1b shows the variation of grain boundary energy with mis-orientation angle mapped onto a stereographic triangle with the convention for representing cubic metals. The vertices of the triangle represent the three principal orientation of the cubic system. The color bar corresponds to the GB energies between 600 mJ/m^2 and 1400 mJ/m^2 which represents the GB database for the three symmetric tilt axes of niobium. The observed trends of the grain boundary energy with mis-orientation angle are comparable to the previously reported values [40].

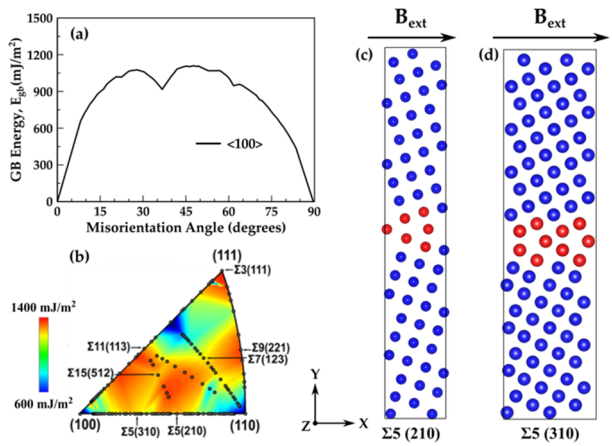

Figure 1: Grain boundary energy (E_{gb}) represented as a function of (a) mis-orientation angle and (b) polar and azimuthal angles for <100> STGBs in Nb. Schematic of externally applied magnetic field (B_{ext}) along the grain boundary plane of (c) Σ5(210) and (d) Σ5(310) GBs in Nb. Atoms are colored according to the common neighbor analysis, where blue and red circles represent bcc and GB atoms, respectively.

Due to the size constraints of first-principles methods, smaller supercells with one periodic length along the GB and few atomic planes (25-35 atomic planes)

ISBN: 978-3-95450-211-0 doi:10.18429/JACoW-SRF2019-TUP056

perpendicular to the GB plane were obtained from the bi-crystal simulation cell of MD calculations. The smaller supercell of the grain boundary was relaxed within DFT framework. The *k* point mesh 6x1x14 was used for Σ5 (210) GB supercells, selected after extensive *k* point sampling, based on the convergence studies. The atoms were relaxed with 10^{-6} eV energy tolerance while maintaining a constant volume and shape of the supercells and with negligible interactions across the periodic images.

RESULTS AND DISCUSSION

The first step towards understanding the flux trapping behavior at different GBs in niobium is to determine the effect of external magnetic field on pure single crystal niobium. It is very well known that niobium is paramagnetic above its superconducting transition temperature and superconducting in nature below T_c. Hence, there is no flux trapping in niobium and the externally applied magnetic field is completely expelled from the material as also observed in our flux trapping simulations. Next, we examine the effect of grain boundaries on flux trapping in niobium using the first-principles and FP-LAPW methods.

To examine the role of grain boundaries on magnetic flux trapping in niobium, the external magnetic field was applied along the GB plane parallel to x-axis of the simulation cell, as illustrated in Figs. 1(c) and 1(d). The trapped or residual magnetic flux density (B_r) due to the presence of defects in niobium was calculated from the remnant magnetic moment (M) as:

$$B_r = \frac{M\mu_0}{V} \qquad (4)$$

where V is volume of the supercell and μ_0 is the permeability of vacuum ($4\pi \times 10^{-7}$ H/m). The applied field decreased gradually to zero at the end of all self-consistent loops and a residual magnetic moment was observed in the GB simulation cells. For instance, a residual magnetic moment of $0.54\mu_B$ was observed in the Σ5 (210) grain boundary. The magnitude of trapped flux was calculated from the residual moment and volume of the simulation cell using Eq. 4, given in Table I. These results are in good agreement with the cold rolled niobium bi-crystal samples where premature flux penetration was observed to occur at 8-20 mT [41].

Table 1: The Magnitude of Trapped Magnetic Flux at Different Grain Boundaries in Niobium

Flux trapping at Nb grain boundary			
Grain Boundary	Volume ($Å^3$)	Magnetic moment (μ_B)	Trapped Flux (mT)
Σ5 (210)	1098.5	0.54	5.74
Σ5 (310)	1535.9	2.00	15.17

An external magnetic field generally engages with both the electron spin and the electronic orbital current in a metallic system. Further, the interaction of magnetic field with different defects can lead to crystalline magnetic anisotropy, magneto-volume effects and difference in electromagnetic state between the grain boundary and the grain interior [42]. Therefore, examination of the electronic structure can play a crucial role in elucidating the underlying mechanisms associated with flux trapping behavior of defects in niobium. The partial and orbital decomposed DOS for different Bader atoms of the grain boundaries were obtained from VASP to determine their localized effect on flux trapping behavior and elucidate the underlying mechanisms associated with flux trapping behavior of defects in niobium. The response of a material to an external source depends on the nature of atomic bonding between the atoms which is associated with the atomic charge distribution [43,44]. Bader's quantum theory of atoms in molecules defines atoms, bonds and chemical structure of the material as a function of the electron density in the system [45]. The charge obtained from the first-principles calculations was separated and determined for each atom using the Bader charge analysis. The DOS curve below the Fermi level (0 eV) represents the occupied states (bonding states); whereas, the curve above the Fermi level represents the unoccupied states (antibonding states) [46,47]. All the electronic density of states calculations were performed using the tetrahedron smearing method with Blöchl corrections within DFT framework.

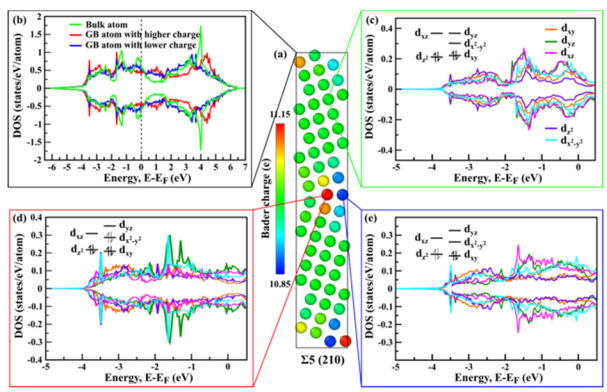

Figure 2: (a) Bader charge analysis for Σ5 (210) STGB in Nb. Atoms are colored according to the atomic Bader charge. (b) Partial DOS curves for different atoms selected based on Bader charge analysis of Σ5 (210) STGB. Orbital decomposed DOS curves for (c) bulk atom, grain boundary atom with charge (d) accumulation and (e) depletion respectively below the Fermi level in Σ5 (210) STGB.

As an illustration, the orbital and partial DOS are shown for the Bader atoms of Σ5 (210) GB (Fig. 2). The partial DOS for the niobium atoms away from Σ5 (210) grain boundary, and at the grain boundary with accumulated and depleted charge respectively were found to be different from each other (Fig. 2b). Additional states were observed below the Fermi level corresponding to

ISBN: 978-3-95450-211-0 doi:10.18429/JACoW-SRF2019-TUP056

electron accumulation in the DOS curve of grain boundary atom with higher Bader charge as compared to the atoms away from grain boundary (Fig. 2d). The accumulated electrons occupy $d_{x^2-y^2}$ orbitals in addition to d_{yz} and d_{xy} orbitals already occupied by the original *4d* electrons (Fig. 2d). On the other hand, the peaks below the Fermi level diminished in the DOS curve of grain boundary atom with lower Bader charge as compared to the bulk atoms indicating towards electron reduction at the grain boundary atom (Fig. 2e). The spin-up and spin-down DOS curves are symmetric for the grain boundary atoms as well as for the atoms away from grain boundary and there is no net magnetic moment in the bi-crystal simulation cell. However, the degeneracy of t_{2g} and e_g states, in un-defected niobium, is lifted due to the presence of grain boundaries. Furthermore, the valence charge transfer around the defects can lead to localization of electrons, resulting in significantly different magnetic properties of defects as compared to the bulk and enhancing tendency of niobium towards magnetism in the presence of external magnetic field.

CONCLUSIONS

In summary, the present work provides a theoretical point of view to understand the interaction of external magnetic field with grain boundaries and its effect on the magnetic properties of niobium via first-principles methods. Equilibrium grain boundary structures were obtained using DFT methods and the external magnetic field was applied within the FP-LAPW code formulation. Further, the electronic structure of defects was determined using density of states and Bader charge analysis within first-principles framework to illustrate the underlying mechanism of interactions between external magnetic field and defects in niobium. Charge redistribution and splitting of *d* states in the defect region suggest towards their significantly different magnetic properties and non-paramagnetic behavior as compared to bcc niobium. Different electronic structure of defects as compared to bulk niobium indicates to a magnetized state in the presence of an external magnetic field thereby promoting flux trapping at defects in niobium.

ACKNOWLEDGMENTS

This work was supported by the US Department of Energy (Award Numbers DE-SC0009962 and DE-SC0009960). We thank Peter Lee and Shreyas Balachandran from the National High Magnetic Field Laboratory, Florida State University for helpful suggestions and discussions.

REFERENCES

[1] P. Dhakal, G. Ciovati, and G. R. Myneni, "Role of thermal resistance on the performance of superconducting radio frequency cavities," *Phys. Rev. Accel. Beams*, vol. 20, no. 3, p. 032003, 2017.

[2] P. Garg, S. Balachandran, I. Adlakha, P. J. Lee, T. R. Bieler, and K. N. Solanki, "Revealing the role of nitrogen on hydride nucleation and stability in pure niobium using first-principles calculations," *Supercond. Sci. Technol.*, vol. 31, no. 11, p. 115007, 2018.

[3] W. Meissner and R. Ochsenfeld, "Ein neuer Effekt bei Eintritt der Supraleitfähigkeit," *Naturwissenschaften*, vol. 21, no. 44, pp. 787–788, 1933.

[4] J. Knobloch and H. Padamsee, "Flux trapping in niobium cavities during breakdown events," presented at the Proc. 8th Workshop on RF Superconductivity, Abano Terme, Italy, 1997, p. 337.

[5] C. Vallet *et al.*, "Flux trapping in superconducting cavities," in *Proc. 3rd European Particle Accelerator Conf. (EPAC'92)*, Berlin, Germany, Mar. 1992, pp. 1295-1298.

[6] P. Dhakal, G. Ciovati, P. Kneisel, and G. R. Myneni, "Enhancement in Quality Factor of SRF Niobium Cavities by Material Diffusion," *IEEE Trans. Appl. Supercond.*, vol. 25, no. 3, pp. 1–4, 2015.

[7] P. Garg, I. Adlakha, S. Balachandran, T. Bieler, P. Lee, and K. Solanki, "Role of Nitrogen on Hydride Nucleation in Pure Niobium by First Principles Calculations," in *Proc. 18th Int. Conf. RF Superconductivity (SRF'17)*, Lanzhou, China, Jul. 2017, pp. 741-745.

[8] A. Gurevich, "Superconducting radio-frequency fundamentals for particle accelerators," *Rev. Accel. Sci. Technol.*, vol. 5, pp. 119–146, 2012.

[9] A Grassellino and A Romanenko and D Sergatskov and O Melnychuk and Y Trenikhina and A Crawford and A Rowe and M Wong and T Khabiboulline and F Barkov, "Nitrogen and argon doping of niobium for superconducting radio frequency cavities: a pathway to highly efficient accelerating structures," *Supercond. Sci. Technol.*, vol. 26, no. 10, p. 102001, 2013.

[10] T. Kubo, "Flux trapping in superconducting accelerating cavities during cooling down with a spatial temperature gradient," *Prog. Theor. Exp. Phys.*, vol. 2016, no. 5, 2016.

[11] P. Dhakal, G. Ciovati, and G. R. Myneni, "A path to higher Q0 with large grain niobium cavities," *ArXiv Prepr. ArXiv12056736*, 2012.

[12] S. Huang, T. Kubo, and R. Geng, "Dependence of trapped-flux-induced surface resistance of a large-grain Nb superconducting radio-frequency cavity on spatial temperature gradient during cooldown through T c," *Phys. Rev. Accel. Beams*, vol. 19, no. 8, p. 082001, 2016.

[13] C. Benvenuti *et al.*, "Study of the surface resistance of superconducting niobium films at 1.5 GHz," *Phys. C Supercond.*, vol. 316, no. 3, pp. 153–188, May 1999.

[14] D. C. Ford, L. D. Cooley, and D. N. Seidman, "First-principles calculations of niobium hydride formation in superconducting radio-frequency cavities," *Supercond. Sci. Technol.*, vol. 26, no. 9, p. 095002, Sep. 2013.

[15] J. Knobloch, "The 'Q disease' in Superconducting Niobium RF Cavities," *AIP Conference Proceedings*, vol. 671, pp. 133–150, 2003.

[16] P. Dhakal *et al.*, "Effect of high temperature heat treatments on the quality factor of a large-grain superconducting radio-frequency niobium cavity," *Phys. Rev. Spec. Top.-Accel. Beams*, vol. 16, no. 4, p. 042001, 2013.

[17] S. Aull, O. Kugeler, and J. Knobloch, "Trapped magnetic flux in superconducting niobium samples," *Phys. Rev.*

ISBN: 978-3-95450-211-0 doi:10.18429/JACoW-SRF2019-TUP056

Spec. Top. - Accel. Beams, vol. 15, no. 6, p. 062001, Jun. 2012.

[18] A. DasGupta, C. Koch, D. Kroeger, and Y. Chou, "Flux pinning by grain boundaries in niobium bicrystals," *Philos. Mag. B*, vol. 38, no. 4, pp. 367–380, 1978.

[19] B. Cai, Y. Chou, *and* A. D. Gupta, "Flux pinning by symmetrical grain boundaries in niobium bicrystals," *Philos. Mag. B*, vol. 55, no. 1, pp. 55–66, 1987.

[20] Z.-H. Sung *et al.*, "Development of low angle grain boundaries in lightly deformed superconducting niobium and their influence on hydride distribution and flux perturbation," *J. Appl. Phys.*, vol. 121, no. 19, p. 193903, May 2017.

[21] B. Khanra, "Flux pinning by grain boundaries in anisotropic superconducting materials," *Phys. Status Solidi B*, vol. 72, no. 1, pp. 303–308, 1975.

[22] L. Vinnikov, E. Zasavitskii, and S. Moskvin, "Critical currents in niobium bicrystals," *Zh Eksp Teor Fiz*, vol. 83, no. 6, pp. 2225–2236, 1982.

[23] C. Pande and M. Suenaga, "A model of flux pinning by grain boundaries in type-II superconductors," *Appl. Phys. Lett.*, vol. 29, no. 7, pp. 443–444, 1976.

[24] G. Kresse and J. Hafner, "Norm-conserving and ultrasoft pseudopotentials for first-row and transition elements," *J. Phys.* Condens. *Matter*, vol. 6, no. 40, p. 8245, 1994.

[25] G. Kresse and J. Furthmüller, "Efficient iterative schemes for ab initio total-energy calculations using a plane-wave basis set," Phys. *Rev. B*, vol. 54, no. 16, p. 11169, 1996.

[26] P. E. Blöchl, "Projector augmented-wave method," *Phys. Rev. B*, vol. 50, no. 24, p. 17953, 1994.

[27] H. J. Monkhorst and J. D. Pack, "Special points for Brillouin-zone integrations," *Phys Rev B*, vol. 13, no. 12, pp. 5188–5192, Jun. 1976.

[28] S. Sharma *et al.*, "First-Principles Approach to Noncollinear Magnetism: Towards Spin Dynamics," *Phys. Rev. Lett.*, vol. 98, no. 19, p. 196405, May 2007.

[29] H. Jin *et al.*, "Phonon-induced diamagnetic force and its effect on the lattice thermal conductivity," *Nat Mater*, vol. 14, no. 6, pp. 601–606, Jun. 2015.

[30] J.-Y. Yang, S.-Y. Yue, and M. Hu, "Bidirectional effect of magnetic field on electronic thermal transport of metals from all-electron first-principles calculations," *Phys. Rev. B*, vol. 94, no. 23, Dec. 2016.

[31] S. Plimpton, "Fast parallel algorithms for short-range molecular dynamics," *J. Comput. Phys.*, vol. 117, no. 1, pp. 1–19, 1995.

[32] M. Rajagopalan, I. Adlakha, M. A. Tschopp, and K. N. Solanki, "Energetics of Hydrogen Segregation to α-Fe Grain Boundaries for Modeling Stress Corrosion Cracking," *JOM*, vol. 69, no. 8, pp. 1398–1403, Aug. 2017.

[33] I. Adlakha, M. A. Bhatia, M. A. Tschopp, and K. N. Solanki, "Atomic scale investigation of grain boundary structure role on intergranular deformation in aluminium," *Philos. Mag.*, vol. 94, no. 30, pp. 3445–3466, Oct. 2014.

[34] M. A. Bhatia and K. N. Solanki, "Energetics of vacancy segregation to symmetric tilt grain boundaries in hexagonal closed pack materials," *J. Appl. Phys.*, vol. 114, no. 24, p. 244309, Dec. 2013.

[35] I. Adlakha, P. Garg, and K. N. Solanki, "Revealing the atomistic nature of dislocation-precipitate interactions in Al-Cu alloys," *J. Alloys Compd.*, vol. 797, pp. 325–333, Aug. 2019.

[36] M. Rajagopalan, M. A. Bhatia, M. A. Tschopp, D. J. Srolovitz, and K. N. Solanki, "Atomic-scale analysis of liquid-gallium embrittlement of aluminum grain boundaries," *Acta Mater.*, vol. 73, pp. 312–325, Jul. 2014.

[37] K. N. Solanki, M. A. Tschopp, M. A. Bhatia, and N. R. Rhodes, "Atomistic Investigation of the Role of Grain Boundary Structure on Hydrogen Segregation and Embrittlement in α-Fe," *Metall. Mater. Trans. A*, vol. 44, no. 3, pp. 1365–1375, Mar. 2013.

[38] M. A. Tschopp, K. N. Solanki, F. Gao, X. Sun, M. A. Khaleel, and M. F. Horstemeyer, "Probing grain boundary sink strength at the nanoscale: Energetics and length scales of vacancy and interstitial absorption by grain boundaries in $\ensuremath{\alpha}$-Fe," *Phys. Rev. B*, vol. 85, no. 6, p. 064108, Feb. 2012.

[39] E. Wachowicz and A. Kiejna, "Effect of impurities on grain boundary cohesion in bcc iron," *Comput. Mater. Sci.*, vol. 43, no. 4, pp. 736–743, 2008.

[40] D. Singh and A. Parashar, "Effect of symmetric and asymmetric tilt grain boundaries on the tensile behaviour of bcc-Niobium," *Comput. Mater. Sci.*, vol. 143, pp. 126–132, Feb. 2018.

[41] P. Lee *et al.*, "Grain boundary flux penetration and resistivity in large grain niobium sheet," *Phys. C Supercond.*, vol. 441, no. 1–2, pp. 126–129, 2006.

[42] T. Watanabe, S. Tsurekawa, X. Zhao, and L. Zuo, "Grain boundary engineering by magnetic field application," *Viewp. Set No 40 Grain Bound. Eng.*, vol. 54, no. 6, pp. 969–975, Mar. 2006.

[43] P. Garg, M. A. Bhatia, and K. N. Solanki, "Uncovering the influence of metallic and non-metallic impurities on the ideal shear strength and ductility of Ti: An ab-initio study," *J. Alloys Compd.*, vol. 788, pp. 413–421, Jun. 2019.

[44] P. Garg, I. Adlakha, and K. N. Solanki, "First-Principles Investigation of the Effect of Solutes on the Ideal Shear Resistance and Electronic Properties of Magnesium," in *Magnesium Technology 2019*, 2019, pp. 231–237.

[45] D. Carballo-Córdova, M. Ochoa-Lara, S. Olive-Méndez, and F. Espinosa-Magaña, "First-principles calculations and Bader analysis of oxygen-deficient induced magnetism in cubic BaTiO3− x and SrTiO3− x," *Philos. Mag.*, vol. 99, no. 2, pp. 181–197, 2019.

[46] P. Garg, I. Adlakha, and K. N. Solanki, "Effect of solutes on ideal shear resistance and electronic properties of magnesium: A first-principles study," *Acta Mater.*, vol. 153, pp. 327–335, Jul. 2018.

[47] P. Garg, M. A. Bhatia, S. N. Mathaudhu, and K. N. Solanki, "Solute Effect on Strength and Formability of Mg: A First-Principle Study," in *Magnesium Technology 2017*, 2017, pp. 483–489.